Radiationless resonant Raman scattering interpretation of argon photoion yields measured in coincidence with K-LL Auger decay

G. Bradley Armen, Jon C. Levin, and Ivan A. Sellin
Department of Physics, University of Tennessee, Knoxville, Tennessee 37996
(Received 10 July 1995)

Measurements of argon photoion yields obtained in coincidence with K-$L_{2,3}L_{2,3}$ Auger emission as a function of incident photon energy across the K-shell threshold are reported. These results are interpreted within the framework of lowest-order scattering theory, which describes the virtual creation and decay of $1s$-hole states. Cross sections for the production of singly ionized spectator Auger states $[2p^2]np$ and the doubly ionized $[2p^2]$ states are calculated using nonrelativistic Hartree-Fock wave functions and their physical interpretation is discussed. When the behavior of the np spectator electron during and after the subsequent Auger cascade that fills the two core $2p$ holes is taken into account, excellent agreement with experiment is obtained. The mechanism for loss of the np electron in this cascade is shown to be a final Auger decay in which the np electron participates and np shake-off is found to be negligible.

PACS number(s): 32.80.Hd, 32.80.Fb, 32.80.Rm

I. INTRODUCTION

The dynamics of photoionization just above and below an ionization threshold is a complex phenomenon [1], in which the correlated behavior of the atomic electrons plays an important role. When the incident-photon energy is tuned near an inner-shell threshold, excitation and decay cannot, in general, be treated as separate events, but must be considered as occurring together through a single second-order process [2].

The essence of such behavior can be studied in detail by examining the energy distribution of the ejected particles, i.e., Auger electrons [3] or photons [4,5]: line shapes and relative intensities supply information on differential cross sections and thus the details of the dynamics [6,7]. On the other hand, general features, such as the behavior of total cross sections, can be revealed by studying the charge distribution of the various ions produced as a consequence of the primary ionization event [8]. A complication inherent in any such scheme is the overwhelming number of final states that can result. In principle, maximum information can only be extracted through the measurement in coincidence of all possible features of all the ejected particles and remnant ion. Although this ideal can only be approached to a limited degree, practical coincidence experiments can be employed to expose very specific aspects of the whole.

In this work threshold photoionization of the argon K shell is examined through the production of ionic charge states measured in coincidence with the emission of K-$L_{2,3}L_{2,3}$ Auger electrons. Because the Auger coincidence constraint effectively selects the first step of the decay cascade, the distribution of charge states is dramatically simplified. Equally important, it is this first ''step'' that must be treated in a unified manner with the excitation. The coincident ion yield provides a useful measure of the cross section for this process and is employed to separate some of the distinctive aspects of the problem. Additionally, theoretical understanding of the various threshold phenomena encountered have only recently begun to coalesce into a unified viewpoint, and the experimental results are reexamined within the context of radiationless resonant Raman scattering (RRRS) [2,9,10], where photon absorption and Auger-electron emission are treated as a single scattering event. This examination puts into a different light many of the aspects of previous experiments that are sometimes viewed as disjoint, most notably spectator Auger emission and photoelectron recapture by postcollision interaction (PCI).

The experimental results reported in this work are refinements of a previous study [8]. The more recent data have smaller statistical uncertainty and provide measurements at a greater variety of incident-photon energies across the K-shell threshold. The experimental method and results are reviewed in Sec. II.

Section III pertains to the theoretical treatment of the primary excitation-decay process. This process can be thought of as the photoexcitation of an inner-shell $1s$ electron accompanied by K-LL Auger emission. In this loose manner of thinking, the ''photoelectron'' can either escape from the atom or remain bound in a Rydberg orbital. Because near threshold there are many indistinguishable routes to arrive at a given final state, the calculation of the probability of such events is a coherent sum of amplitudes for all possible paths. RRRS provides such a quantitative description in terms of virtual intermediate states associated with a $1s$ vacancy. An outline of the general theory of RRRS is presented and its adaptation to the current experimental setup is discussed.

Hartree-Fock calculations of the RRRS cross sections for the above-mentioned processes are presented in Sec. IV. The cross section for the various spectator Auger states, in which the atom is left in a state Ar $[2p^2]np$ (square brackets denote holes) after the primary excitation-decay, is the topic of Sec. IV A. These spectator cross sections are shown to display the effects of interference between the various paths possible, but for lower np states a physical interpretation of the cross sections in terms of spectator shake and PCI recapture is possible and is discussed. Once the total spectator cross section is established, the cross section for double ionization to the Ar $[2p^2]$ states can be extracted from the total probability. This is the subject of Sec. IV C where the partitioning of

the total cross section into double- and single-ionization cross sections is demonstrated. PCI-induced recapture is shown to delay the onset of double ionization until the incident photon energy is well above (several K-shell widths) threshold. The calculated total cross section is compared with the measured total ion yield and satisfactory agreement is achieved.

While RRRS predicts the probability of the primary excitation-decay processes, subsequent Auger decay fills the two $2p$ holes created in the primary event. To complete the analysis, the fate of np Rydberg electrons populated in the RRRS process during and after the subsequent cascade is considered within the framework of a simple model. This model, presented in Sec. IV B, allows for both shake-off and np participator Auger decay as a mechanism for np electron loss. Our model indicates that essentially all np loss is due to a final participator decay step. Combining the RRRS excitation probability with this cascade analysis, the measured Ar^{3+} yield is shown to be in excellent agreement with our theoretical predictions

Finally, relative ion yields are discussed in Sec. IV D. Again the Ar^{3+} results are shown to be in excellent agreement with theory. The relative yield of Ar^{5+} is overestimated, however, and some of the limitations of our cascade model are discussed in this connection.

II. EXPERIMENT

The experiment was conducted on the National Institute of Standards and Technology beam line X-24A at the National Synchrotron Light Source. Details of the beamline and experiment have been discussed previously ([8,11,12] and references therein) and only a brief outline is presented here.

Synchrotron radiation that was energy selected by a Si [111] double-crystal monochromator (bandpass 0.32–0.64 eV at $h\nu \approx 3206$ eV [12]) was focused near the tip of a grounded stainless-steel gas jet. This needle was positioned in the extraction region of a time-of-flight (TOF) analyzer utilized for ionic charge-state analysis. Both the needle and TOF analyzer were attached to an XYZ manipulator that permitted positioning of the needle in the source volume of a commercial cylindrical-mirror electron-energy analyzer (CMA). The TOF analyzer consisted of a series of field and drift regions of total length ≈ 5 cm designed to maintain space focusing. The photoions where detected by a pair of chevroned microchannel plates.

In the electron-ion coincidence measurements, an Auger-electron event from the CMA was employed as a start signal to a time-to-amplitude converter (TAC), which was then stopped by the TOF photoion signal. The CMA was set to accept electrons of kinetic energy 2660 eV, with a wide electron-energy bandpass (≈ 20 eV). Output from the TAC, after pulse height analysis, resulted in a coincident TOF spectrum from which relative ion yields could be extracted.

In order to study in detail ion yield as a function of photon energy in the vicinity of the K-shell edge, it was necessary to monitor the energy calibration of the x-ray monochromator. This calibration was maintained by bracketing each coincidence TOF spectrum with a measurement of the total ion yield as a function of photon energy. The $1s$-$4p$ resonance, a prominent feature of the ion-yield ''edge,'' was employed as reference. To allow comparison of the ion yields at different photon energies, the total counts from each coincidence TOF spectrum was normalized to a standard total ion-yield spectrum taken with high statistics.

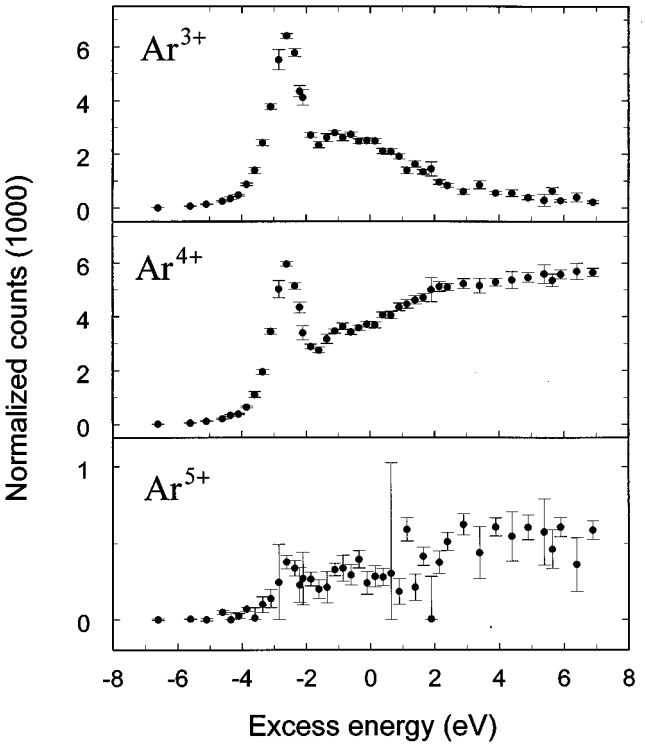

FIG. 1. Charge-state abundances of argon ions measured in coincidence with K-$L_{2,3}L_{2,3}$ Auger emission as a function of excess energy, the incident-photon energy relative to the K-shell threshold. At each photon energy, the counts have been normalized to a standard total ion yield (Fig. 6) to correct for changes in beam intensity and sample time between measurements at different energies.

The experimental results are displayed in Fig. 1 for the three charge states observed. For consistency with later discussion, the incident-photon energy is indicated relative to the K-shell threshold (excess energy).

III. THEORY

A. Overview

When monochromatic x rays are tuned to energies near the Ar K-shell threshold, there is a wealth of excitation modes that lead to the emission of one or more electrons [6] or electrons and photons [4]. The ejection of such particles can be envisaged as the Auger or fluorescence decay of resonantly excited states associated with the temporary creation of a $1s$ hole. The general process has come to be termed radiative and radiationless resonant Raman scattering ([2,9,10] and references therein).

The present work is concerned with the detection of Ar ions in coincidence with electrons emitted with kinetic energies near the K-$L_{2,3}L_{2,3}$ Auger energy. Near threshold, the relevant processes are

$$\mathrm{Ar}+\omega \rightarrow \mathrm{Ar}^{1+}[2p^2]np+\varepsilon_S l_A \qquad (1a)$$

and

$$\mathrm{Ar}+\omega\rightarrow\mathrm{Ar}^{2+}[2p^2]+\varepsilon_P l_P+\varepsilon_A l_A\,. \tag{1b}$$

For photon energies ω near the K-shell threshold, the *direct* excitation of such final states [e.g., $2p$ shake-up (1a) or shake-off (1b) accompanying $2p$ ionization] is of negligible importance. Instead, the amplitude for such transitions is derived from the Auger decay of the virtual, singly excited intermediate states $\mathrm{Ar}^{0+}\ [1s]mp$ and $\mathrm{Ar}^{1+}\ [1s]\tau p$.

Transitions of the type (1a) are only observed for photon energies near or just below the K-shell edge, and result in ''spectator'' Auger lines with energies ε_S near that of the K-$L_{2,3}L_{2,3}$ transition. From (1a) it is clear that the spectator Auger energy should exhibit a linear dependence on the incident-photon energy. In this sense, the spectator Auger line is seen to be a resonantly enhanced photoelectron (satellite) line.

Transition (1b) results in the ejection of two electrons, an Auger electron with energy ε_A near the nominal K-$L_{2,3}L_{2,3}$ energy, and a photoelectron whose energy ε_P is near the excess energy $E_{\mathrm{exc}}=\omega-I_K$, where I_K is the ionization energy of a $1s$ electron. For low excess energies, the slow photoelectron is still in the vicinity of the atom when the fast Auger electron is emitted. In this case PCI between the two electrons results in line-shape distortions and shifts [6,7]. In general, the photoelectron is shifted to lower energies, while the Auger electron line shifts to higher. For larger excess energies, PCI effects disappear [13–16] (at least in the angle-averaged sense [17,18]) and the process evolves into the conventional two-step diagram K-$L_{2,3}L_{2,3}$ decay.

Spectator Auger decay and PCI Auger emission are often not regarded as distinct: In the semiclassical view the escaping photoelectron can be recaptured by the ion at low E_{exc}, due to the sudden change in screening seen by the photoelectron when the Auger electron is ejected. In this semiclassical view, spectator states arise from two separate processes: the excitation of the $1s$ electron to a bound np state, which passively acts as a spectator during the core Auger decay, and the PCI-induced recapture of the photoelectron [19,20]. From a quantum-mechanical viewpoint, the intermediate state through which the system passes cannot be observed and it is the amplitudes of all such ''paths'' that must be added. Only when a particular resonance state is energetically distant from all others can the process be treated in the single-resonance approximation [21–23]. In the case of the Ar K-shell threshold, where even the largest energy separation is only twice the natural width, coherence between alternate paths is of crucial importance.

B. Spectator states

When excited by monochromatic incident radiation, the line shape of the ejected spectator Auger electrons is approximately a Lorentzian function whose width is determined only by the lifetime of the final state [23]. The average spectator energy is $\bar{\varepsilon}_S=\omega-I_{LL,n}$, where $I_{LL,n}$ is the ionization energy of the final ionic state $\mathrm{Ar}\,[2p^2]np$. This expression can be rewritten in terms of the excess energy, nominal Auger energy $\bar{\varepsilon}_A==I_K-I_{LL}$, and the ionization energy i_n^{++} of the np electron relative to the Ar $[2p^2]$ core as $\bar{\varepsilon}_S=E_{\mathrm{exc}}+\bar{\varepsilon}_A+i_n^{++}$. For photon energies *below* threshold by an amount i_n^{++}, the emitted spectator Auger line will have a kinetic energy equal to that of the diagram Auger line.

Threshold effects, such as PCI and RRRS have previously been explained within the context of scattering theory [24,3,21,22]. After integration over emitted electron energy, we take the cross section for the production of Ar $[2p^2]np$ states as

$$\sigma_{np}^{+}(E_{\mathrm{exc}})=\tfrac{2}{3}\pi\alpha\omega\Gamma_{K\text{-}LL}\left|\langle np|\tau_0\rangle\right|^2 \tag{2}$$

in atomic units. Here α is the fine-structure constant and Γ_{K-LL} is the partial rate for the diagram K-$L_{2,3}L_{2,3}$ Auger decay [24].

The resonant enhancement of the spectator line in the photon energy region near the K-shell binding energy is dictated by the overlap

$$\langle np|\tau_0\rangle=\sum_{m>3}\frac{\langle np|mp\rangle A(mp)}{E_{\mathrm{exc}}+\tau_m+i\Gamma_K/2}+\int_0^{\infty}\frac{\langle np|\tau p\rangle A(\tau p)}{E_{\mathrm{exc}}-\tau+i\Gamma_K/2}d\tau, \tag{3}$$

where the intermediate-state photoexcitation amplitude $A(xp)$ $(x=m,\tau)$ is

$$A(xp)=\langle[1s]xp(^1P)\|\mathbf{D}^{(1)}\|(^1S)\rangle. \tag{4}$$

Further discussion of this function is relegated to Sec. III D.

Each term of the above overlap (3) can be loosely interpreted as an amplitude for the photoexcitation of a K-shell electron into an intermediate state, either bound (mp) or continuous (τp), followed by shake or recapture to the np orbital as the core ejects an Auger electron. Each of the intermediate state orbitals mp and τp are determined in the presence of the $\mathrm{Ar}^{1+}\ [1s]$ core, while the final state np orbital is determined in the presence of the $\mathrm{Ar}^{2+}\ [2p^2]$ core. The (positive) ionization energy of the bound intermediate-state mp electron with respect to the $\mathrm{Ar}^{1+}\ [1s]$ core is denoted τ_m. The K-shell total width Γ_K reflects the lifetime of the virtual states.

Implicit in the above formulas is a summation over all spectator multiplet states that are unresolved in the experiment. The presence of the mp spectator electron ''splits'' the $[2p^2](^1D)$ parent level into the three final ionic states in LS coupling: $[2p^2](^1D)np(^2P)$, $[2p^2](^1D)np(^2D)$, and $[2p^2](^1D)np(^2F)$. Hartree-Fock calculations reveal that the energy splitting between the three (^1D) spectator Auger lines is quite small [less than 0.2 eV for $n=4$, in comparison to the (^1S)-(^1D) diagram splitting $\approx$10 eV [25]]. If the acceptance of the electron spectrometer is set wide enough to also include the $[2p^2](^1S)np(^2P)$ states, the implied summation yields the factor Γ_{K-LL}, the diagram K-$L_{2,3}L_{2,3}$ partial decay rate. This result rests upon certain assumptions about the factorization of the many-electron matrix elements involved and that the np spectator electron does not drastically alter any of the core electrons relative to the diagram case.

In a coincidence experiment in which the acceptance of the electron spectrometer is wide in comparison to the spectator shifts and dispersion, the probability of excitation to one of the Ar $[2p^2]np$ spectator states will be proportional to the cross section of Eq. (2). However, since the $[2p^2]$ vacancy is itself unstable, the ion will decay further. This subsequent decay is treated in the two-step approximation, so

that the cascade process proceeds from one well-defined (distinguishable) state to the next. This assumption is partially justified by the longer lifetimes of the cascade states and by the emission of Auger electrons with characteristic energies at each stage. For an experiment that detects ions of a charge state q, the cross section for the creation of a specific np state must be weighted by the probability P_{np}^{q+} that subsequent cascade decay ends in a charge state q. These probabilities are discussed in the Sec. IV B. Furthermore, the cross section must be convoluted with the spectral function. $N(\omega-\omega_0)$ and a sum must be performed over all states. The experimental yield of ions resulting from the creation of the spectator Auger states *alone* is thus proportional to

$$Y^{q+}(E_{\rm exc})=\sum_{n>3} P_{np}^{q+}\int d\omega\sigma_{np}^{+}(E_{\rm exc})N(\omega-\omega_0). \quad (5)$$

C. Total ion yield

The cross section for the double-ionization process (1b) can be written [26,6] as

$$\sigma^{++}(E_{\rm exc})=\tfrac{2}{3}\pi\alpha\omega\int_0^{E_{\rm exc}+\bar{\varepsilon}_A} d\varepsilon\left|\langle\varepsilon p|\tau_0\rangle\right|^2\Gamma_{K\text{-}LL}(\varepsilon_A), \quad (6)$$

which is simply an integration over the PCI-distorted photoelectron line shape. The Auger energy ε_A is connected to that of the photoelectron by conservation of total energy: $\varepsilon+\varepsilon_A=E_{\rm exc}+\bar{\varepsilon}_A$. While the direct computation of the PCI line shape gives good agreement with experimentally observed line shapes [6,7] and with semiclassical line shapes at larger excess energies [14], direct calculation of Eq. (6) is laborious, typically involving the computation of several thousand continuum functions [3,6,26]. If the line shape itself is not desired an alternate approach can be employed.

An excellent approximation is to assume that the partial Auger rate is constant over the photoelectron line shape and can thus be removed from the integral. The total cross section is then defined as

$$\sigma_{\rm total}=\sigma^{++}+\sum_{n>3}\sigma_{np}^{+}. \quad (7)$$

By calculating the total cross section, σ^{++} can be extracted by subtraction if the total spectator cross section is known. Assuming that the final-state np and εp orbitals form a complete set, the total cross section becomes

$$\sigma_{\rm total}(E_{\rm exc})=\frac{2}{3}\pi\alpha\omega\Gamma_{K\text{-}LL}\left[\sum_{m>3}\frac{|A(mp)|^2}{(E_{\rm exc}+\tau_m)^2+\Gamma_K^2/4}+\int_0^{\infty}\frac{|A(\tau p)|^2}{(E_{\rm exc}-\tau)^2+\Gamma_K^2/4}d\tau\right]. \quad (8)$$

So long as there is no observation of the final ionic state, the distribution of intensity among the final states ''after'' the K-$L_{2,3}L_{2,3}$ decay is of no concern. The total ion yield is thus expressible in terms of excitations to intermediate states only. Analysis of the total absorption edge [27] along the same lines is also valid. However, the use of Eq. (8) to infer properties intrinsic to the final state may be misleading [8,28] since the individual terms of the equation carry no real physical significance.

In Eqs. (6) and (2), the multiplicative constant has been chosen [26] to ensure the high-energy limit

$$\sigma_{\rm total}\underset{E_{\rm exc}\gg\Gamma_K}{\longrightarrow}\frac{\Gamma_{K\text{-}LL}}{\Gamma_K}\left[\frac{4}{3}\pi^2\alpha\omega|A(E_{\rm exc}\,p)|^2\right]=\frac{\Gamma_{K\text{-}LL}}{\Gamma_K}\sigma_K(E_{\rm exc}), \quad (9)$$

where $\sigma_K(E_{\rm exc})$ is the conventional K-shell photoionization cross section [29]. For large excess energies the ion yield factorizes allowing the usual the two-step interpretation: the K-shell photoionization cross section multiplied by the branching ratio for diagram K-$L_{2,3}L_{2,3}$ decay.

D. Photoexcitation amplitude

The calculation of the intermediate-state photoexcitation amplitudes $A(xp)(x=m,\tau)$ of Eq. (4) merits some discussion. Many calculations ([26,30–33] and references therein) have been performed in attempts to obtain agreement with experimental measurements of the absolute Ar photoabsorption cross section [34]. In the single-configuration frozen-core model, and using the length form of the dipole operator, the amplitude limits to [29]

$$A(xp)\rightarrow-\sqrt{2}\int_0^{\infty}P_{xp}rP_{1s}dr. \quad (10)$$

If atomic relaxation is to be included by employing separate nonorthogonal sets of orbitals for the ground and excited states, the expression for $A(xp)$ becomes more complicated, involving combinations of dipole and monopole single-particle excitations [30,32]. Often it suffices to use the frozen-core expression (10) as an approximation, but substituting the relaxed xp orbital. In the case of single-configuration Hartree-Fock (HF) calculations for Ar it has been demonstrated [26,30–32] that the full relaxation expression must be used.

Our approach is to employ relaxed single-configuration HF wave functions for all states, specifically the Ar ground and Ar $[1s]xp(^1P)$ states. There is, however, still some latitude for confusion concerning the orthogonality between orbitals that *comprise* a given many-electron state. Cooper [32] has performed HF photoexcitation calculations in the length gauge, while experimenting with orthogonality constraints between the orbitals that comprise the $[1s]xp$ state, for both the configuration average and (^1P) state. For bound-state excitation he finds that the oscillator strengths [proportional to $|A(mp)|^2$, $m=4,5$] are decreased by a factor of 0.80 when the orthogonality between final-state orbitals is enforced. In the nonorthogonal model he finds that his computed photoabsorption cross sections agree well with the relativistic calculations of Tulkki and Åberg [26], lying about 5% below the measured values. Although Cooper did not calculate the ionization cross section for models in which orthogonality was strictly enforced, he has predicted from the scaled oscillator strengths for excitation that a HF calculation employing strict orthogonality requirements would underestimate the cross section.

TABLE I. Comparison of relaxed single-configuration Hartree-Fock photoionization cross sections (kb) when final-state orbital orthogonality is rigorously maintained (O) or ignored completely (NO). For each excess energy, the calculations are listed in the length (L), velocity (V), and acceleration (A) gauges.

	σ_K (kb)					
	O			NO		
E_{exc} (eV)	L	V	A	L	V	A
3	69.3	71.6	75.7	85.3	72.3	75.8
10	67.7	69.6	73.3	82.4	70.3	73.4
30	64.3	65.3	68.4	75.9	66.0	68.6
70	61.3	61.4	64.0	69.5	62.1	64.1
110	59.2	58.9	61.2	65.6	59.5	61.3

In fact, our HF photoionization calculations in the length gauge do differ from Cooper's results by a factor of about 0.81 near threshold, verifying his reasoning. Our results for the bound-state oscillator strengths agree well with those of Cooper's orthogonal results. We have used two independent sets of programs for our calculations: The first is a modified continuum package [35] working in conjunction with the bound-state multiconfiguration HF package of Froese-Fischer [36] and the second is a photoionization program [37] employing the bound-state HF code of Mayers and O'Brien [38].

As a test, we relaxed the orthogonality requirement for the final-state orbitals in two stages. First, orthogonality between the continuum τp orbital and the core $2p$ and $3p$ orbitals was removed by ignoring the relevant Lagrange multipliers. This resulted in cross sections that differed only slightly from the full-orthogonality calculation. The calculation was repeated, but additionally removing the orthogonality constraints between the core orbitals. In consequence, the $1s$, $2s$, and $3s$ final-state core orbitals become slightly nonorthogonal [32]. The resulting length-gauge photoionization cross section was increased from the full-orthogonality case, agreeing with Cooper's values.

Our photoionization calculations were also performed in the velocity and acceleration gauges. Using these forms of the dipole operator, the neglect of final-state orthogonality requirements causes little change in the cross sections. Table I lists our values of σ_K in all three gauges for several values of excess energy, with final-state orthogonality fully enforced (O) or completely ignored (NO). The large change in cross section due to the nonorthogonality of the final-state core orbitals is a feature of the length-gauge calculations only.

In what follows, we choose to employ the (^1P) amplitude calculated with full relaxation while strictly enforcing orthogonality of the final-state orbitals through the use of Lagrangian multipliers. This approach is the most consistent to follow within the single-configuration approximation. Also, the agreement between length, velocity, and acceleration gauges is much better than that obtained using the nonorthogonal final-state basis, in which the improved value of the length-form result may only be fortuitous.

There remains some uncertainty as to comparisons with other calculations. Cooper has noted the agreement of his NO calculations with the relativistic calculations of Tullki and Åberg [26] and suggests that orthogonality may not have been maintained in their calculation. The early work of Sukhorukov *et al.* [30] also quotes the larger cross section, greater than 80 kb for the first 30 eV above threshold. Saha [33] has obtained excellent agreement with the near-threshold data employing a nonrelativistic HF calculation in which relaxation, along with other forms of electron correlation, has been included by configuration-interaction techniques. Saha [33] mentions agreement of test calculations with the relaxed calculations of both Cooper [32] and Tukki and Åberg [26], but does not elaborate.

IV. RESULTS AND DISCUSSION

A. Spectator cross sections

In this section, details of the calculation of the spectator cross sections for Eq. (2) as well as the physical insight gained from the procedure are discussed. As outlined in Sec. III D, the amplitude for excitation to intermediate states, both bound and continuous, was computed using full relaxation between wave functions described by HF calculations of the Ar ground and Ar $[1s]xp(^1P)$ states. The final state np orbitals derive from HF calculations with a $[2p^2]$ core configuration; the Ar $[2p^2](^1D)np(^2F)$ states were optimized since this is the most probable final state of the np multiplet. HF calculations were performed for $n=4-10$.

The bound mp intermediate states where calculated for $m=4-14$. For a given n, the intermediate-state summation for $m>14$ was completed using a quantum-defect fit to both $\langle np|mp\rangle$ and $A(mp)$ with the intermediate-state quantum defect $\delta_i=1.662$. The continuous intermediate states were computed on a radial mesh out to a maximum radius of 500 a.u. Since both the overlaps $\langle np|\tau p\rangle$ and the excitation amplitudes $A(\tau p)$ are smooth functions of τ, they need be calculated at only a few energies ranging from 0.1 up to 100 eV. The product $\langle np|\tau p\rangle A(\tau p)$ was then spline interpolated onto an energy mesh over which the ''Lorentzian'' integration was performed. For $\tau>100$ eV, the overlap-amplitude term was extrapolated by a power-law fit and the integration continued analytically. This tail correction generally altered the total integral by no more than 1%.

The total K-shell width has been taken as $\Gamma_K=0.66$ eV [39] and the K-$L_{2,3}L_{2,3}$ partial width to be $\Gamma_{K-LL}=0.33$ eV [40]. This latter choice, which amounts to an overall scaling factor, implies a K-$L_{2,3}L_{2,3}$ branching ratio of 50%. These values are the result of relativistic Dirac-Hartree-Slater calculations in intermediate coupling, including some configuration interaction. A branching ratio of 46% and a K-shell width of 0.64 eV is obtained from single-configuration nonrelativistic HF calculations [41].

Figure 2 displays the spectator cross sections calculated as functions of the excess energy near the K-shell threshold ($E_{\text{exc}}=0$). The first few intermediate-state resonance energies, for which $E_{\text{exc}}=-\tau_m$, are indicated by vertical lines in Fig. 2 (b) just above the ordinate axis. The cross sections are presented in kilobarns (kb) and the vertical scale of the plots is changed from panel to panel for clarity.

Figure 2(a) shows the $4p$ cross section, calculated in the length (solid line), velocity (dotted line), and acceleration (dash-dotted line) gauges. There is a large cross-section enhancement at the $4p$ resonance energy and a smaller one near the $5p$ resonance energy. The $4p$ resonance can be

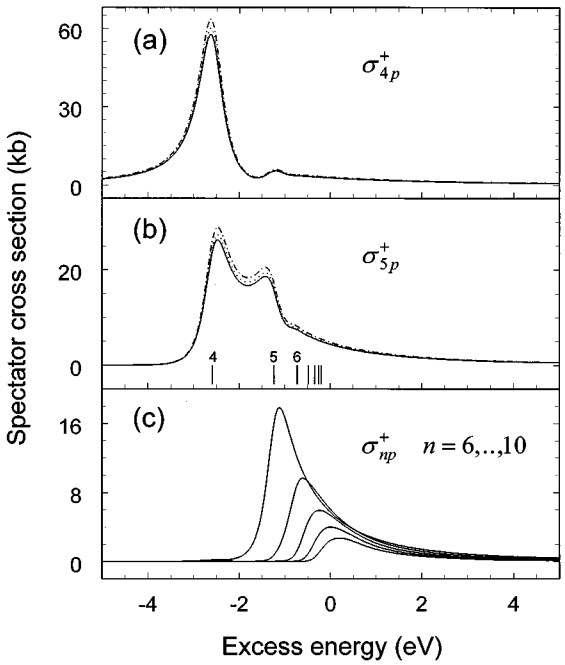

FIG. 2. Calculated cross sections for the excitation of singly ionized Ar $[2p^2]np$ spectator Auger states. The first few intermediate-state resonance energies are indicated by vertical lines in (b) just above the ordinate axis. The vertical scale is magnified progressively from (a) to (c). Length, velocity, and acceleration gauge results are indicated in by solid, dotted, and dash-dotted lines, respectively. For a specific final np state, the enhancement of the cross section near the various resonance energies can be interpreted in terms of shake transitions of intermediate-state mp orbitals and photoelectron recapture.

loosely thought of as a pure-spectator transition [21]; the $1s$ electron is excited into the $m=4$ intermediate state and maintains its occupancy during the core Auger transition. Similarly, the small peak at the $5p$ resonance energy can be ascribed to shake-down; the $1s$ electron is excited to an $m=5$ intermediate state, which shakes to the $n=4$ orbital during the core transition. The broad tail at higher excess energies is due to shake-down from higher bound intermediate states and from the continuum (recapture). Because the Ar K-shell width is comparable to the resonance energy spacing, these processes cannot be treated as distinct, even for the lowest-lying levels. The amplitudes from the various terms interfere and the resulting cross section is not a sum of individual Lorentzian functions weighted by excitation and shake factors. Even for excess energies far below threshold, the amplitude for recapture plays a significant role, particularly so off resonance: For $E_{\rm exc}=-5$ eV, 22% of the real part of the amplitude (which is dominant) is due to recapture, which can be thought of as increasing the cross section (constructively) by about 44%.

Figure 2(b) shows a similar plot for the $5p$ cross section. The maximum production probability for the $5p$ spectator state occurs at the resonance for $4p$ intermediate-state production. This can be envisaged as the shake-up of an $m=4$ electron to $n=5$ during the core transition. The cross-section enhancement at the $5p$ resonance is then ''pure''spectator and the tail at larger excess energies is due to shake-down and recapture. The $5p$ cross section thus exhibits the general trend [21,42–46] that, for higher Rydberg orbitals that experience and increase in screening charge, shake-up is the dominant mechanism.

For larger n, the resonance energies crowd together and the spectator cross sections take on broad features. Figure 2(c) shows the $n=6$ (largest) through $n=10$ (smallest) spectator cross sections. Only the length-gauge calculations are indicated for clarity; the agreement between the various gauges is similar to that of the $4p$ and $5p$ cases. Again, the dominance of intermediate-state shake up is revealed, i.e., the cross section for producing the $6p$ spectator state has a maximum for photon energies near the $5p$ resonance energy. For larger n, the amplitude for recapture from the continuum plays an increasingly dominant role, so that for $n=10$, the amplitude is largely due to this ''mechanism.''

Numerical calculations can be carried out for only a limited number of spectator states. For $n>10$, the computation of the spectator cross sections must be estimated by other means. The function $|\tau_0\rangle$, viewed as a function of radial distance, is exponentially damped [6,21] and this damping becomes more pronounced for lower $E_{\rm exc}$. It should then be expected that the overlap of this function with a highly extended final-state np orbital would show the usual quantum-defect $(n-\delta_f)^{-3/2}$ scaling, where $\delta_f=1.382$ is the *final-state* quantum defect. Numerical experimentation with the $n=7$–10 cross sections does show the expected $(n-\delta_f)^{-3}$ scaling; however, there is also an overall shift of the function to larger $E_{\rm exc}$ as n increases. This shift is found to be linearly dependent on i_n^{++}, with a constant of proportionality equal to 0.85.

The origin of this shift can be traced to an interesting scaling property for the recapture overlaps. For hydrogenic orbitals, numerical experimentation reveals that

$$n^3\langle np,Z_B|\varepsilon p,Z_C\rangle^2 \approx n'^3\langle n'p,Z_B|\varepsilon' p,Z_C\rangle^2 \quad \text{with} \quad \varepsilon'=\varepsilon+\beta(i_n^{Z_B}-i_{n'}^{Z_B}). \quad (11)$$

For the choice $Z_B=2$ and $Z_C=1$, it is found that $\beta\approx 0.850$ and is insensitive to changes in energy or in n and n'. The above relation can be derived from a Taylor-series expansion in energy, once the bound orbitals have been renormalized per unit energy [47]. The shifts of the quantum-defect scaled cross sections arise from the fact that recapture is the dominance contribution to the amplitude and that the overlaps in the amplitude integral scale as in Eq. (11) with the final-state quantum defect included. The cross section for excitation to spectator states of $n>10$ was thus extrapolated from the $n=10$ cross section with appropriate scaling and shifting.

As with all such quantum-defect summations, the cross section for $n>10$ is significant. Figure 3 shows the total spectator cross section, including the contribution for large n obtained by scaling and shifting. The dashed line indicates the contribution for the final states $n=4$–10. The total spectator cross section is seen to extend roughly 1 eV above threshold before dropping away smoothly at higher excess energies.

The foregoing discussion indicates how the spectator cross sections can be loosely interpreted in terms of skake up or shake down of the intermediate-state mp electron to a final bound np orbital when the core undergoes Auger decay.

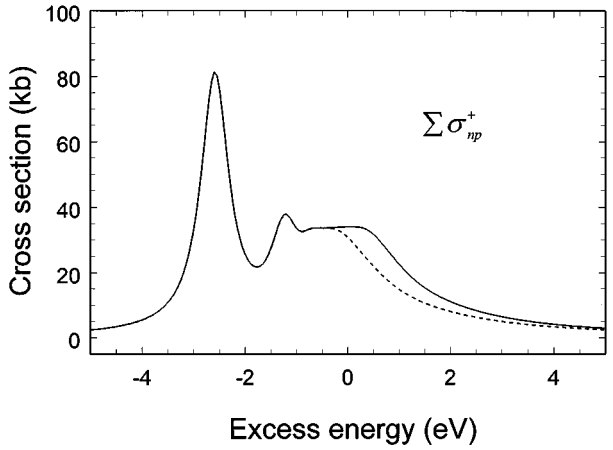

FIG. 3. Total cross section for production of the Ar $[2p^2]np$ spectator Auger final states as a function of excess energy (solid line). The dashed line indicates the sum of cross sections computed numerically for $n=4-10$, the summation over larger n being completed by quantum-defect scaling. Only the length-gauge results are shown.

With this intuitive picture in mind, the question naturally arises as to shake-off of the mp electron during the core decay. Since this ''process'' results in a final-state continuum electron ($mp\rightarrow\varepsilon p$) and an ejected Auger electron, it is indistinguishable from the ''Auger'' ($\tau p\rightarrow\varepsilon p$) double-ionization process. The cross section for ''spectator shake-off'' is thus included in the calculation of σ^{++}[Eq. (6)]. Since the shake-off amplitude [identified by the terms involving the $\langle\varepsilon p|mp\rangle$ overlaps implicit in Eq. (6)] must be added to the Auger amplitude (the $\langle\varepsilon p|\tau p\rangle$ terms), there is no unique way to define a shake-off cross section. In practice, the PCI line-shape function $|\langle\varepsilon p|\tau_0\rangle|^2$ could be calculated [6] as a function of photoelectron energy ε and a shake-off intensity defined (arbitrarily) by removing a photoelectron ''peak'' from the continuous distribution. Such ambiguities arise because intuitive expressions such as spectator shake-up, shake-down, and shake-off describe physical processes only in the limit that a resonance becomes isolated, i.e., a single intermediate state is traversed.

B. Cascade effects and the Ar^{3+} yield

The preceding subsection dealt with the probability of creating the spectator Auger states $[2p^2]np$. For insight into the ionic charge states observed in coincidence with Auger emission, the subsequent decay of the $[2p^2]$ core must be considered. The simplest such charge state to analyze is Ar^{3+}, which can only result if the excited np electron remains bound to the ion as the two $L_{2,3}$ holes bubble up via $L_{2,3}$-MM decay to form four holes in the M shell. Decay routes involving $L_{2,3}$-M radiative decay are ruled out since the L-shell fluorescence yields are negligible [48].

To interpret the Ar^{3+} yield, the probabilities P^{3+}_{np} of Eq. (5) are needed. The computation of such probabilities requires accurate knowledge of the branching ratios of all possible decay paths. We invoke the simplest possible model for cascade decay in order to make estimates. Two key assumptions are made.

(i) Apart from accompanying shake transitions, the np electron plays no role in the filling of the two $L_{2,3}$ holes. This is in keeping with the usual assumptions that participator rates are negligible when there are core Auger paths open. The process can then be thought of as following one of the possible decay paths $[2p^2]np\rightarrow[2p][MM]n'p\rightarrow[MMMM]n''p$, where the final $[MMMM]$ configuration is stable against further Auger decay.

(ii) Once the two $L_{2,3}$-MM transitions have occurred, the remaining $n''p$ electron is free to experience valence-multiplet or inner-valence participator Auger decay [49–53] if the transition if energetically possible. This presumes that the rates for any open participator Auger channels will be large in comparison to those of the radiative channels. This adds a final cascade $[MMMM]n''p\rightarrow[MMMMM]+e^-$, resulting in Ar^{4+}. It is the stability of the $n''p$ orbital against such decay that determines the Ar^{3+} yield.

With the above model for cascade decay in mind, we write

$$P^{3+}_{np}=\sum_{\gamma} p_{\gamma}\bar{S}_{\gamma}(n) \tag{12}$$

for the probability that an np spectator state cascades to a final ionic charge state of $q=+3$. Here p_{γ} is the probability that a given four-hole valence configuration γ ($\gamma=M_1^2M_{2,3}^2$, $M_1M_{2,3}^3$ or, $M_{2,3}^4$) will result from the core cascade and $S_{\gamma}(n)$ is the average ''sticking'' probability of the spectator electron. This is the probability that a spectator electron starting in the level n will remain bound to the final core γ. This probability accounts for the electron surviving shake-off during both core Auger transitions and ending in a level that is stable against final participator Auger decay. The average is taken over all LS substates of a given core γ.

In estimating p_{γ}, the branching ratios for argon $L_{2,3}$-MM decay are employed as a starting point. These are taken as $L_{2,3}$-M_1M_1 (0.035), $L_{2,3}$-$M_1M_{2,3}$ (0.141), $L_{2,3}$-$M_{2,3}M_{2,3}$ (0.671), $L_{2,3}$-$M_{2,3}^3nl^*$ (0.046), and $L_{2,3}$-$M_{2,3}^3$ (0.107) from ratios of the experimental Auger intensities of Werme, Bergmark, and Siegbahn [54] and Carlson and Krause [55]. The latter two transitions account for shake-up of a $3p$ electron to nl^* ($4s$ or $4d$) levels or $3p$ shake-off accompanying the Auger decay. In the former case, the shake-up probability is likely underestimated since there are many unassigned lines in addition to the $4s$ and $4d$ satellites [54].

From the above branching ratios, relative partial decay rates are assigned. By modifying these relative rates to account for partially filled shells [56], modified branching ratios can be assigned and the probabilities for decay to various final core states can be traced. Starting from an $L_{2,3}^2$ double-hole state, the *core* cascade ends in four-hole valence states 77.4% of the time: $M_1^2M_{2,3}^2$ (0.098), $M_{1,2}M_{2,3}^3$ (0.255), and $M_{2,3}^4$(0.421). The remaining 22.6% of all core decays result in M^5 or M^5nl^* core states. Since it is assumed that doubly excited ($nl^*n''p$) states will decay by ejection of at least one electron, these latter core states are of no further interest in the discussion of Ar^{3+} yields.

The average sticking probability is taken to be

TABLE II. Stable Ar^{4+} states possible in the single-configuration Hartree-Fock approximation. For each four-hole valence configuration γ, populated from the decay of Ar $L_{2,3}^2$ with probability p_γ, the LS multiplets are listed. The energy of each state relative to that of the lowest is given in eV. $n''_{\min}$ is the minimum quantum number a Rydberg electron bound to the $(\gamma LS)^{4+}$ core can have for which participator Auger decay $(\gamma LS)^{4+}n''l \rightarrow (\gamma' L' S')^{4+}+e^-$ is energetically possible.

Configuration	γ	p_γ	LS	$E_{\rm rel}$ (eV)	$n''_{\min}$
Ar $[3p^4]$	$M_{2,3}^4$	0.421	^3P	0	stable
			^1D	2.3	11
			^1S	5.6	7
Ar $[3s^1 3p^3]$	$M_1 M_{2,3}^3$	0.255	^5S	7.9	6
			^3D	15.6	5
			^3P	17.8	5
			^1D	24.0	4
			^3S	24.8	4
			^1P	26.2	4
Ar $[3s^2 3p^2]$	$M_1^2 M_{2,3}^2$	0.098	^3P	36.7	4
			^1D	38.9	4
			^1S	42.2	4

$$\bar{S}_\gamma(n)=\frac{1}{g_\gamma}\sum_{LS} g_{\gamma LS}\left[\sum_{n''<n''_{\min}(\gamma LS)} f(n,n'')\right]. \qquad (13)$$

Here $g_{\gamma LS}=(2L+1)(2S+1)$ is the degeneracy of a given LS substate of the core configuration γ and g_γ is the total degeneracy of that configuration. The shake transition probability $f(n,n'')$ describes the probability of an np electron being shaken to the $n''p$ orbital after experiencing two increases in central charge Z. This probability is summed for all final-n'' levels that *do not* lead to participator decay. This is characterized by a minimum value of $n'', n''_{\min}(\gamma LS)$, for which at least one participator Auger channel *is* energetically allowed from the γLS configuration.

The $n''_{\min}(\gamma LS)$ were determined as follows. First, HF calculations for all the γLS Ar^{4+} cores were performed and their energies relative to the lowest state $M_{2,3}^4(^3P)$ were determined. For each state γLS, the relative energy ($E_{\rm rel}$) was compared to the average ionization energies ($i_{n''}^{4+}$) of $n''p$ electrons in the presence of an Ar^{4+} core. From this comparison, a minimum value for n'' could be determined so that $E_{\rm rel}-i_{n''}^{4+}>0$. Hence, for all $n''\geqslant n''_{\min}(\gamma LS)$ there exists at least one core state $\gamma' L' S'$ for which the participator Auger transition $(\gamma LS)n''p\rightarrow(\gamma' L' S')+e^-$ is energetically allowed. Table II summarizes the results. It is seen that the $(M_1^2 M_{2,3}^2)n''$ states can decay for all values of n'', the $(M_1 M_{2,3}^3)n''$ states for all or fairly low n'' values, but that the $(M_{2,3}^4)n''$ states are stable until fairly large values of n'' are reached.

The shake transition probability is calculated within the sudden approximation, where a sudden change in central charge is experienced by the Rydberg electron during each core transition. Summing over the probabilities for all possible intermediate (distinguishable) paths yields

TABLE III. Average sticking probability $\bar{S}_\gamma(n)$, the probability that a spectator electron starting in the level $[2p^2]np$ will remain bound after two successive $L_{2,3}$-MM Auger transitions to the final core γ. When weighted with the probabilities of decay to each final core, the total probability P_{np}^{3+} of producing an Ar^{3+} ion is obtained.

	$S_\gamma(n)$			
n	$M_{2,3}^4$	$M_1 M_{2,3}^3$	$M_1^2 M_{2,3}^2$	P_{np}^{3+}
4	0.999	0.669	0	0.591
5	0.932	0.120	0	0.423
6	0.932	0.023	0	0.398
7	0.932	0.009	0	0.394
8	0.924	0.004	0	0.390
9	0.705	0.002	0	0.297
10	0.671	0.001	0	0.283

$$f(n,n'')=\sum_{n'} |\langle np,Z=2|n'p,Z=3\rangle|^2 \times|\langle n'p,Z=3|n''p,Z=4\rangle|^2. \qquad (14)$$

In principle, this probability should be a function of the particular route taken for the decay. However, there is only one path that leads to $M_{2,3}^4$, which is of primary interest $(L_{2,3}^2\rightarrow L_{2,3}M_{2,3}^2\rightarrow M_{2,3}^4)$, and so has been computed using configuration-average HF Ar $[2p,3p^2]n'p$ and $[3p^4]n''p$ wave functions. The sum was carried out for $n=4$–10 and $n', n''=4$–18.

As found previously [21], the most likely fate of the spectator electron is to be shaken up by one or two units of n during each increase in core change. Truncation of the intermediate summation to $n'\leqslant 18$ was thus not a large source of error for $n\leqslant 10$. The loss of the spectator electron due to shake-off during the core Auger decay is implicitly accounted for in the above sum through the completeness of the $n'p$ and $n''p$ bases. An upper bound for shake-off can be established for each stage by subtracting the total computed shake probability from unity. The remainder reflects the probability for shake to orbitals higher than $n=18$, or to shake off. In all cases, this upper bound was found to be less than 0.2%. Several test calculations, in which the shake-off probability was calculated directly, confirmed this result. Thus shake-off, at least within the context of the sudden approximation, is of negligible importance in the loss of the spectator electron. Instead, the loss is found to be entirely due to participator Auger decay and the quantities $n''_{\min}(\gamma LS)$ play the crucial role in Eq. (13). For the most part, ion-yield experiments (including this work) fail to distinguish between these two mechanisms [57]; however, very recent work on Ne addresses this issue [58].

Table III displays the final results for the sticking probabilities and the total probabilities P_{np}^{3+}. The probability that the spectator electron remains with the ion is seen to decrease with increasing n. This trend is a composite of two processes: For a given starting value of n, the most likely outcome of the two sudden changes in screening is to increase n and it is more likely for a participator Auger channel to be energetically allowed the larger this final n value is.

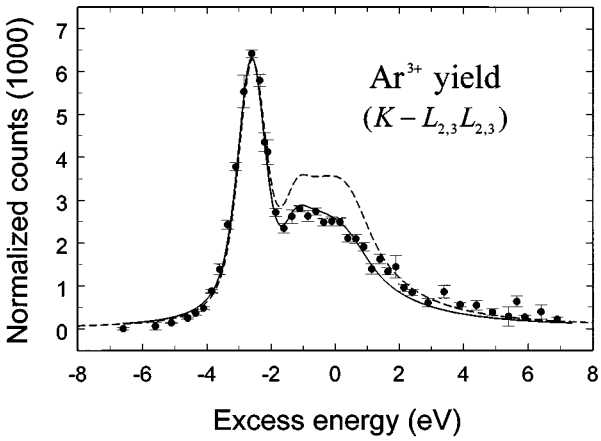

FIG. 4. Ar^{3+}-ion yield in coincidence with Ar K-$L_{2,3}L_{2,3}$ emission, compared with the theoretical spectator cross section (solid line), modified to account for the loss of the np spectator electron during the two subsequent cascade decays filling the $L_{2,3}$ holes. This modified cross section has been convoluted with a Gaussian spectral function of width 0.635 eV and adjusted by an overall constant to best fit the data. The dashed line indicates the distribution expected if spectator loss is ignored.

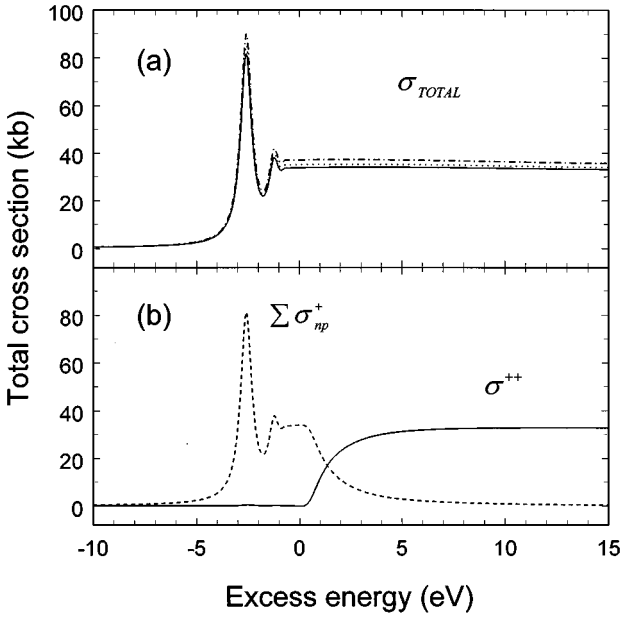

FIG. 5. (a) Total cross section for the emission of an electron with kinetic energy "near" the diagram Ar K-$L_{2,3}L_{2,3}$ energy, calculated from the sum rule Eq. (8) in the length, velocity, and acceleration gauges. (b) Upon subtraction of the total spectator cross section (dashed line) the cross section for producing the doubly ionized Ar $[2p^2]$ states is obtained (solid line) in the length gauge. PCI-induced recapture of the photoelectron results in spectator final states, delaying the onset of double-ionization intensity until approximately 1.4 eV above threshold.

Finally, the theoretical prediction of the Ar^{3+}-ion yield as a function of photon energy can be compared with the experimental measurement. To do so, effects due to the spectral width of the incident-photon energy distribution [23] must be included by convolution. The spectral function was assumed to be Gaussian with a full width at half maximum (FWHM). Γ_ω. Using the values of P_{np}^{3+} from Table III, the theoretical prediction for the 3+ yield [Eq. (5)] was fitted to the data with an overall scaling parameter. For $n>10$ it was assumed that $P^{3+}(np)=P^{3+}(10p)$. In these fits, the energy scale was fixed by setting the $4p$ resonance peak at $E_{\rm exc}=-2.6$ eV, in keeping with the present theoretical results (-2.59 eV) and in close agreement with Breinig *et al.* [27] (-2.72 eV). Fits were performed for a variety of spectral widths and the best fit (minimum χ^2) was obtained with $\Gamma_\omega=0.635$ eV. This value is consistent with the expected photon-energy resolution at $\omega\approx 3206$ eV.

Figure 4 shows the comparison between the data and the theoretical prediction for the production of Ar^{3+} ions in coincidence with the emission of K-$L_{2,3}L_{2,3}$ electrons. The solid line is the one-parameter fit (scale factor) of the theory, which accounts for the subsequent loss of the spectator electrons during the cascade decay of the hole. The agreement with theory is excellent. The above-threshold production of Ar^{3+}, analogous to the same effect observed just above the Ar L-shell threshold [19,20], is seen to persist for several Γ_K above the K-shell edge. For comparison, a dashed line is included that shows the distribution expected if the subsequent spectator loss is either ignored or assumed to be independent of n.

C. Total ion yield

The total cross section for the production of an ion of any charge, coincident with the emission of a K-$L_{2,3}L_{2,3}$ electron, is given by Eq. (8). Since the relaxed amplitudes for intermediate-state excitation and ionization (Sec. III D) are employed in the calculation of the spectator cross sections, it is a simple matter to sum and integrate them with the appropriate Lorentzian weights. Summation over the high-n bound states is performed using the usual (intermediate-state) quantum-defect extension of the amplitudes and resonance energies. The results of these calculations are shown in Fig. 5(a). Again, results in the length, velocity, and acceleration gauges are indicated (lower to higher curves, respectively).

For above-threshold excitation ($E_{\rm exc}>0$) the total cross section can be compared with the two-step photoionization value $(\Gamma_{K-LL}/\Gamma_K)\sigma_K$ of Eq. (9). At threshold, the latter cross section is larger by about 3%. This PCI-induced reduction of the photoionization cross section near threshold has been noted by Tullki and Åberg [26]. It can be traced (mathematically) to two competing effects: Factoring out the almost-constant amplitude from the integral of Eq. (8) yields an integral over a portion of a Lorentz function, producing an arc-tangent factor. It is loss of this "Lorentzian area" in the integral that produces the cross-section reduction. For excess energies several eV above threshold, the percent difference between the two results is very well described by the function $\frac{1}{2}-(1/\pi)\tan^{-1}(2E_{\rm exc}/\Gamma_K)$. However, very near threshold this reduction is compensated (but not totally) by intensity from bound large-n intermediate-state excitations.

The cross section for the double-ionization process, in which two electrons are ejected leaving a final $[2p^2]$ state, is obtained by subtracting the total spectator cross section of the last section. This is indicated in Fig. 5(b); the dashed line indicates the total cross section for producing $[2p^2]np$ states and the solid curve shows the difference from the total. The

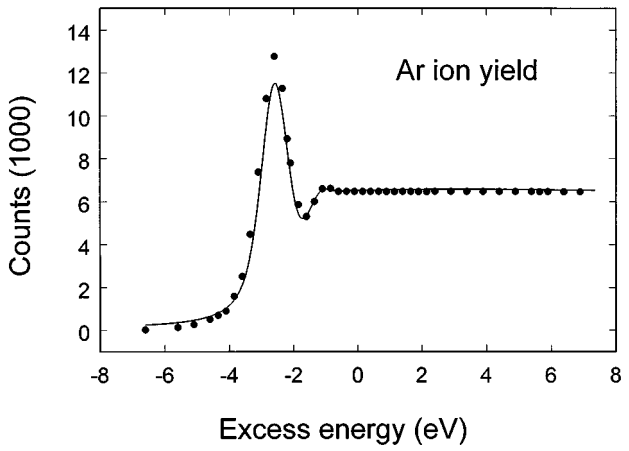

FIG. 6. Comparison of the measured total ion yield with the theoretical total cross section. As in Fig. 4, the cross section has been convoluted with a Gaussian spectral function of width 0.635 eV and adjusted by an overall constant to best fit the data.

difference thus represents the cross section for ejection of two electrons (photoelectron and Auger) during the primary excitation event. For clarity, Fig. 5(b) shows only the length-form result.

It can be seen from Fig. 5(b) that there is a pronounced delay in the onset of the double-ionization edge. This can be viewed as PCI-induced recapture [20] of the slowly moving photoelectron near threshold, forming singly ionized spectator states. For excess energies $E_{\rm exc} \leqslant \Gamma_K$, almost the entire probability goes into the production of spectator states. For larger values of $E_{\rm exc}$ the growing double-ionization cross section σ^{++} tracks the RRRS evolution of the PCI-distorted photoelectron and Auger lines into the familiar two-step K-$L_{2,3}L_{2,3}$ diagram process. For $E_{\rm exc} \approx 1.4$ eV the single- and double-ionization probabilities are equal, supporting the general rule of thumb that ω must be above threshold by at least several Γ_K's before recapture of the photoelectron can be ignored. For a small region at threshold, our values of σ^{++} become slightly negative by as much as 0.3% of the total cross section. This reflects the level of numerical accuracy inherent in our estimation of the large-n spectator cross sections.

This suppression of the diagram intensity near threshold is also in accord with the recent work of Hayaishi *et al.* [59]. In this work, charge-state yields are measured in coincidence with zero-kinetic-energy electrons. They find that the onset of photopeak intensity (Ar^{4+} coincidence) is delayed until the photon energy exceeds threshold by about 1 eV. However, the comparison cannot be pushed too far since our calculation describes the intensity of the entire photopeak as a function of incident energy, while their measurements reflect the zero-energy portion of the (energy-dependent) line shape.

Figure 6 compares the calculated total cross section with the measured total ion yield. The function $\sigma_{\rm total}$ of Fig. 5 has been convoluted with a Gaussian ($\Gamma_\omega = 0.635$ eV) to account for the spectral width of the photon beam. The total yield presented in the figure was not measured in coincidence, but used to normalize the coincidence measurements at different excess energies for variations in beam intensity and sample time. The ratio of the intensity of the $4p$ resonance to the above-threshold region is very sensitive to the spectral function employed. For this reason, the convoluted function was fitted with a scaling factor, using a number of values for Γ_ω. The best fit was achieved for a FWHM of 0.64 eV, which gives a good consistency check against the Ar^{3+} results. Although agreeing well with the data, the $4p$ resonance is slightly under estimated relative to the above-threshold yield, while the low-energy tail is slightly over estimated. Such discrepancies may well be related to the choice of a Gaussian function to represent the spectral distribution.

As expected, the calculated and experimental total-ion yield reproduces the familiar shape of the Ar absorption edge. However, the above-threshold region of the ion yield is quite flat in the first ~ 8 eV above threshold; the experimental yield is flat to statistical uncertainty and the calculation slightly increases by 0.7% from threshold for roughly 3.5 eV and then decreases slowly back to the threshold value again by 8 eV. These results are in contrast to the clear decrease of about 5% over the same range observed in the photon-absorption measurements of Deslattes *et al.* [34].

D. Relative ion yields

In the previous sections it was shown that the lowest-order scattering theory description of RRRS excitation coupled with a simple model for cascade decay provides very good agreement with observed ion yields as functions of excess energy. A further issue to examine is the relative abundance of ions produced in coincidence with the K-$L_{2,3}L_{2,3}$ transition as the photon energy is scanned across threshold. Since they are simple ratios, these abundances are not dependent on any normalization. Because of the K-$L_{2,3}L_{2,3}$ coincidence conditions, the number of charge states observed is greatly reduced [8] from that observed in noncoincidence experiments, with only the three species Ar^{3+}, Ar^{4+} and Ar^{5+} having measurable intensity.

As previously mentioned, the Ar^{3+} states are the most straightforward to examine from a theoretical viewpoint. They can only arise from the decay of the $[2p^2]np$ spectator states to *stable* configurations $[3l^4]n''p$ and their abundances reflect a history of two diagram $L_{2,3}$-MM decays. The present theoretical prediction for the relative yield of Ar^{3+} ions is given by

$$\frac{I(\mathrm{Ar}^{3+})}{I(\mathrm{Ar}^{3+}+\mathrm{Ar}^{4+}+\mathrm{Ar}^{5+})} = \frac{1}{\bar{\sigma}_{\rm total}} \sum_{n>3} \bar{\sigma}^{+}_{np}(E_{\rm exc}) P^{3+}_{np} , \tag{15}$$

where the overbar indicates that the respective cross sections have been convoluted with the experimental spectral function ($\Gamma_\omega = 0.635$ eV). The Ar^{3+} relative yield of Eq. (15) is plotted in Fig. 7, along with the experimental result. The agreement between theory and experiment is again very good, implying that the present model works well, not only for the *relative* values of P^{3+}_{np} (Fig. 4), but also for their absolute magnitudes.

Since the Ar^{3+} relative yield is well described by theory, the abundance of Ar^{4+} and Ar^{5+} is also represented with equal accuracy. A final test is thus to compare one of these last two yields with experiment. The Ar^{5+} yield is chosen since its low probability provides the most stringent trial.

For photon energies more than 3 eV above threshold, the

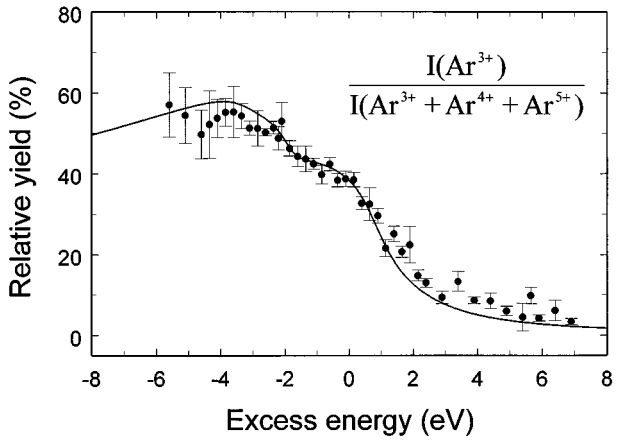

FIG. 7. Measured relative abundance of Ar^{3+} ions detected in coincidence with K-$L_{2,3}L_{2,3}$ electron emission. The solid line indicates the theoretical prediction. The only parameter implicit in the theoretical curve is the width of the incident-photon energy distribution, which is fixed to be consistent with that used in Figs. 4 and 6.

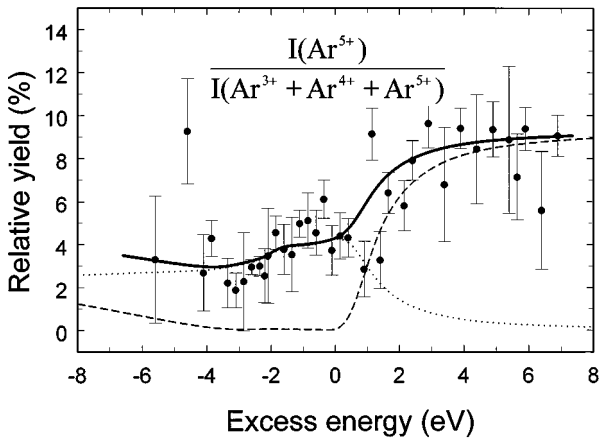

FIG. 8. Measured relative abundance of Ar^{5+} ions detected in coincidence with K-$L_{2,3}L_{2,3}$ electron emission. The solid line represents the best fit of a two-parameter model function [Eq. (16)]. These two parameters apportion to the Ar^{5+} yield $f^{++}=(9.3\pm0.4)\%$ of the double-ionization cross section (dashed line) and $f^{+}=(7.0\pm0.3)\%$ of the spectator cross section (dotted line), which does not contribute to Ar^{3+}.

dominant states created are the doubly ionized $[2p^2]$. Decay of these states during the two successive Auger cascades to Ar^{5+} can only be realized from M-shell shake-off accompanying *one* of the two L-MM decays. A simple estimate can be made: As previously noted, the branching ratio for L-MMM shake-off is taken as $f=0.107$ [55]. A state M^5 can result from L-MMM followed by L-MM or L-MM followed by L-MMM. The expected Ar^{5+} relative yield would then be roughly $2f(1-f)=19.1\%$. When the various branching ratios are adjusted to account for multiple vacancies during the different cascade steps, our model yields a slightly smaller result of 15.5%. These estimates do not include the possible decay of M^5nl^* states by participator Auger processes, an upper bound for which is 6.7% in our model. The experimental ratio is approximately 9% at larger excess energies, so that our model overestimates the high-energy yield by nearly a factor of 2.

For photon energies near or below threshold, where only the $[2p^2]np$ spectator states are excited, the interpretation becomes more difficult. The argument is similar to the above discussion of the $[2p^2]$ decay; however, there is the added complication of determining the probabilities that states $(M^5)np$ or $(M^5nl^*)np$ undergo participator decay. A maximum branching ratio would be equal to the double-ionization case, assuming all np electrons can decay. From the Ar^{3+} case, it is seen that spectator electrons are ionized roughly 50% of the time (Fig. 1). Taking this observation as a guide, it might be concluded that the Ar^{5+} yield below threshold should be about half the above-threshold value. Experimentally this is found to be the case.

With the above comments in mind it is natural to define two probabilities: f^{++}, the probability that a $[2p^2]$ state decays to M^5, and similarly f^{+}, the *average* probability that a spectator state that *does not* decay to Ar^{3+} does result in Ar^{5+}. In terms of these two parameters, the Ar^{5+} relative yield can be expressed in terms of the $Ar^{4+}+Ar^{5+}$ relative populations, which the cascade model does predict well for the spectator case:

$$\frac{I(\mathrm{Ar}^{5+})}{I(\mathrm{Ar}^{3+}+\mathrm{Ar}^{4+}+\mathrm{Ar}^{5+})}=\frac{1}{\bar{\sigma}_{\mathrm{total}}}\left[f^{+}\sum_{n>3}\bar{\sigma}^{+}_{np}(E_{\mathrm{exc}})(1-P^{3+}_{np})+f^{++}\bar{\sigma}^{++}(E_{\mathrm{exc}})\right]. \quad (16)$$

Figure 8 shows the measured relative yield. The solid line is the result of a least-squares fit of Eq. (16) to the data with f^{+} and f^{++} as free parameters. Because of the low yield, the error in these ratios can be quite substantial; only those points with meaningful small error bars are shown. The fitted results are $f^{++}=(9.3\pm0.4)\%$ and $f^{+}=(7.0\pm0.3)\%$. The dashed line shows the contribution from the $[2p^2]$ initial states and the dotted curve indicates the contribution from the decay of the spectator $[2p^2]np$ states.

It is interesting to note that the fitted value of f^{++}, the branching ratio for only one M-shell shake-off in the cascade, is very near 11%, the experimental branching ratio [55] for the decay of a single L-shell hole. This suggests that the L-MMM decay channel is only a feature of the first step in the L^2 decay. While in our model the individual rates for each step (and hence branching ratios) are adjusted to account for multiple M- and L-shell vacancies, the method of adjustment [56] relies only on the recoupling of electrostatic matrix elements. However, the rate for the L-MMM process at the simplest level also relies on an overlap integral, which may be very sensitive to screening effects and is not reflected in statistical arguments. Thus it may well be that LM^2-M^5 is much less probably than L-M^3, beyond what would be expected by the mere lack of two M-shell electrons to participate in the rearrangements.

V. CONCLUSIONS

The near-threshold K-shell ionization of Ar is described in terms of the resonant production of singly and doubly ionized states through the virtual K-LL Auger decay of $[1s]xp$

intermediate states. This interpretation is based on the lowest-order scattering theory description of RRRS.

Production of the singly ionized $[2p^2]np$ spectator Auger states occur mainly below threshold, but the amplitudes for PCI recapture play an important role that dominates for large-n final states. At threshold, the total cross section is almost entirely due to the production of spectator states with $n>10$. By tracing the evolution of a particular np cross section as a function of photon energy, we show how concepts based on the two-step model such as spectator shake-up or shake-down are reflected in the emission probability. At the same time, it is indicated how these cross sections reflect the coherence between paths taken through the various intermediate states.

Above threshold, the doubly ionized $[2p^2]$ states gain intensity. It is seen that PCI effects transfer intensity from the double-ionization cross section to that of the spectator near threshold. The onset of the double ionization is thus shown to be ''delayed'' until the incident photon energy is above threshold by approximately 1.4 eV.

A simple model is introduced to account for the fate of np spectator electrons during the two Auger decays which fill the $[2p^2]$ core holes subsequent to the primary excitation-decay event. It is assumed the np electron plays no role in these two Auger stages, but experiences increases in screening charge during which it is either shaken to other bound orbitals $(n''p)$ or ionized. The probabilities of such are estimated by HF overlaps. Shake-up is found to be the dominant process and shake-off negligible. Once the inner-shell holes have filled, there is a probability that the spectator electron can participate in a further Auger step through a final participator transition. An estimate of the final distribution of M-shell holes and the shake probability of ending in an $n''p$ orbital is employed to predict the probability of such events.

This cascade model, together with the RRRS predictions of initial-state excitation, accounts very well for both the normalized and the relative Ar^{3+} yield as functions of incident-photon energy. By extension, the yield of $Ar^{4+}+Ar^{5+}$ is thus also accounted for. The small Ar^{5+} yield results from the loss of an M-shell electron during *one* of the L-MM cascades and also the loss of the spectator electron if the primary excitation is into a spectator state. The theoretical model is found to overestimate the relative abundance by almost a factor of 2. To describe these results with a higher precision, the cascade model probably requires modification to account for the increase of screening in the higher-order L-MMM cascade channels.

ACKNOWLEDGMENTS

This work was supported by the National Science Foundation. The National Synchrotron Light Source at Brookhaven National Laboratory, Upton, NY is supported by the U.S. Department of Energy (Division of Materials Sciences and Division of Chemical Sciences of the Office of Basic Energy Sciences).

[1] V. Schmidt, Rep. Prog. Phys. **55**, 1483 (1992).
[2] T. Åberg and B. Crasemann, in *Resonant Anomalous X-ray Scattering: Theory and Applications*, edited by G. Materlik, C. J. Sparks, and K. Fischer (North-Holland, Amsterdam, 1994), p. 431.
[3] G. B. Armen, T. Åberg, J. C. Levin, B. Crasemann, M. H. Chen, G. E. Ice, and G. S. Brown, Phys. Rev. Lett. **54**, 1142 (1985).
[4] T. Åberg and J. Tulkki, in *Atomic Inner-Shell Physics*, edited by B. Crasemann (Plenum, New York, 1985), p. 419.
[5] M. A. MacDonald, S. H. Southworth, J. C. Levin, A. Henins, R. D. Deslattes, T. LeBrun, Y. Azuma, P. L. Cowan, and B. A. Karlin, Phys. Rev. A **51**, 3598 (1995).
[6] J. Tullki, G. B. Armen, T. Åberg, B. Crasemann, and M. H. Chen, Z. Phys. D **5**, 241 (1987).
[7] G. B. Armen, J. Tulkki, T. Åberg, and B. Crasemann, Phys. Rev. A **36**, 5606 (1987).
[8] J. C. Levin, C. Biedermann, N. Keller, L. Liljeby, C.-S. O, R. T. Short, I. A. Sellin, and D. W. Lindle, Phys. Rev. Lett. **65**, 988 (1990).
[9] B. Crasemann, Comments At. Mol. Phys. **22**, 163 (1989).
[10] T. Åberg, Phys. Scr. **T41**, 71 (1992).
[11] J. C. Levin, C. Biedermann, N. Keller, L. Liljeby, C.-S. O, R. T. Short, I. A. Sellin, and D. W. Lindle, Nucl. Instrum. Methods Phys. Res. Sect. B **56/57**, 124 (1991).
[12] D. W. Lindle, W. L. Manner, L. Steinbeck, E. Villalobos, J. C. Levin, and I. A. Sellin, J. Electron Spectrosc. Relat. Phenom. **67**, 373 (1994).
[13] G. N. Ogurtsov. J. Phys. B **16**, L745 (1983).
[14] A. Russek and W. Mehlhorn, J. Phys. B **19**, 911 (1986).
[15] M. Borst and V. Schmidt, Phys. Rev. A **33**, 4456 (1986).
[16] G. B. Armen, S. L. Sorenson, S. B. Whitfield, G. E. Ice, J. C. Levin, G. S. Brown, and B. Crasemann, Phys. Rev. A **35**, 3966 (1987).
[17] M. Yu. Kuchiev and S. A. Sheinerman, Zh. Éksp. Teor. Fiz. **90**, 1680 (1986) [Sov. Phys. JETP **63**, 986 (1986)].
[18] G. B. Armen, Phys. Rev. A **37**, 995 (1988).
[19] W. Eberhardt, S. Bernstorff, H. W. Jochims, S. B. Whitfield, and B. Crasemann, Phys. Rev. A **38**, 3808 (1988).
[20] J. Tulkki, T. Åberg, S. B. Whitfield, and B. Crasemann, Phys. Rev. A **41**, 181 (1990).
[21] S. B. Whitfield, J. Tulkki, and T. Åberg, Phys. Rev. A **44**, R6983 (1991).
[22] H. Wang, J. C. Woicik, T. Åberg, M. H. Chen, A. H. Gomez, T. Kendelewicz, A. Mäntykenttä, K. E. Miyano, S. Southworth, and B. Crasemann, Phys. Rev. A **50**, 1359 (1994).
[23] G. B. Armen and H. Wang, Phys. Rev. A **51**, 1241 (1995).
[24] T. Åberg and G. Howat, in *Corpuscles and Radiation in Matter I*, edited by S. Flügge and W. Mehlhorn, Handbuch der Physick Vol. XXXI (Springer, Berlin, 1982), p. 469.
[25] L. Asplund, P. Kelfve, B. Blomster, H. Siegbahn, and K. Siegbahn, Phys. Scr. **16**, 268 (1977).
[26] J. Tulkki and T. Åberg, J. Phys. B **18**, L489 (1985).
[27] M. Breinig, M. H. Chen, G. E. Ice, F. Parente, and B. Crasemann, Phys. Rev. A **22**, 520 (1980).

[28] D. V. Morgan, R. J. Bartlett, and M. Sagurton, Phys. Rev. A **51**, 2939 (1995).
[29] A. F. Starace, in *Corpuscles and Radiation in Matter I* (Ref. [24]), p. 1.
[30] V. L. Sukhorukov, V. V. Demekhin, V. V. Timoshevskaya, and S. V. Larventev, Opt. Spectrosk. **47**, 407 (1979) [Opt. Spectrosc. (USSR) **47**, 228 (1979)].
[31] M. Ya Amusia, V. K. Ivanov, and V. A. Kupchenko, J. Phys. B **14**, L667 (1981).
[32] J. W. Cooper, Phys. Rev. A **38**, 3417 (1988).
[33] H. P. Saha, Phys. Rev. A **42**, 6507 (1990).
[34] R. D. Deslattes, R. E. LaVilla, P. L. Cowan, and A. Henins, Phys. Rev. A **27**, 923 (1983).
[35] G. B. Armen, Ph.D. thesis, University of Oregon, 1985 (unpublished).
[36] C. Froese Fischer, Comput. Phys. Commun. **14**, 145 (1978).
[37] F. P. Larkins (private communication).
[38] D. F. Mayers and F. O'Brien, J. Phys. B **1**, 145 (1968).
[39] M. H. Chen, B. Crasemann, and H. Mark, Phys. Rev. A **21**, 436 (1980).
[40] M. H. Chen, B. Crasemann, and H. Mark, Phys. Rev. A **21**, 442 (1980).
[41] A. G. Kochur, V. L. Sukhorukov, A. I. Dudenko, and Ph. V. Demekhin, J. Phys. B **28**, 387 (1995).
[42] J. A. de Gouw, J. van Eck, J. van der Weg, and H. G. M. Heideman, J. Phys. B **25**, 2007 (1992).
[43] H. Aksela, S. Aksela, J. Tulkki, T. Åberg, G. M. Bancroft, and K. H. Tan, Phys. Rev. A **39**, 3401 (1989).
[44] H. Aksela, O.-P. Sairanen, S. Aksela, A. Kivimäki, A. Naves de Brito, E. Nõmmiste, J. Tulkki, A. Amusmees, S. J. Osborne, and S. Svensson, Phys. Rev. A **51**, 1291 (1995).
[45] M. Meyer, E. v. Raven, B. Sonntag, and J. E. Hansen, Phys. Rev. A **43**, 177 (1991).
[46] J. A. de Gouw, J. van Eck, A. C. Peters, J. van der Weg, and H. G. M. Heideman, J. Phys. B **28**, 2127 (1995).
[47] A. R. P. Rau and T. Heim (private communication).
[48] M. O. Krause, J. Phys. Chem. Ref. Data **8**, 307 (1979).
[49] T. Hayaishi, E. Murakami, A. Yagishita, F. Koike, Y. Morioka, and J. E. Hansen, J. Phys. B **21**, 3203 (1988).
[50] U. Becker, R. Wehlitz, O. Hemmers, B. Langer, and A. Menzel, Phys. Rev. Lett. **63**, 1054 (1989).
[51] G. B. Armen and F. P. Larkins, J. Phys. B **24**, 741 (1991).
[52] G. B. Armen and F. P. Larkins, J. Phys. B **25**, 931 (1992).
[53] U. Becker and R. Wehlitz, Phys. Scr. **T41**, 127 (1992).
[54] L. O. Werme, T. Bergmark, and K. Siegbahn, Phys. Scr. **8**, 149 (1973).
[55] T. A. Carlson and M. O. Krause, Phys. Rev. Lett. **17**, 1079 (1966).
[56] T. Åberg and G. Howat, in *Corpuscles and Radiation in Matter I* (Ref. [24]), Sec. 9γ, p. 521, and references therein.
[57] K. Ueda, E. Shigemasa, Y. Sato, A. Yagishita, M. Ukai, H. Maezawa, T. Hayaishi, and T. Sasaki, J. Phys. B **24**, 605 (1991).
[58] T. Hayaishi, E. Murakami, Y. Morioka, E. Shigemasa, A. Yagishita, and F. Koike, J. Phys. B **28**, 1411 (1995).
[59] T. Hayaishi, E. Murakami, Y. Morioka, E. Shigemasa, A. Yagishita, and F. Koike, J. Phys. B **27**, L115 (1994).